

**Sergey Trofimov**

Keldysh Institute of Applied Mathematics, RAS, Russian Federation, trofimov@keldysh.ru

**Maksim Shirobokov**

Keldysh Institute of Applied Mathematics, RAS, Russian Federation, shirobokov@keldysh.ru

**Anastasia Tselousova, Mikhail Ovchinnikov**

Keldysh Institute of Applied Mathematics, RAS, Russian Federation

Near-rectilinear halo orbits (NRHOs) are periodic orbits that belong to the families of halo orbits around the  $L_1/L_2$  points in a three-body system and have low minimum distances to the smaller primary. NRHOs possess some good dynamical and geometrical properties and are now considered as potential orbits for a near-future crewed deep space station. Recently, intensive investigations have been performed with regard to different aspects of a lunar NRHO mission: Earth-NRHO transfers, station keeping, shadow avoidance, and ground station visibility conditions are deeply studied. At the same time, the important operation of soft lunar landing from the working NRHO is still poorly covered in literature. In this research, we analyze both the direct landing scenario and the option of a transfer from the working NRHO to the intermediate low-perilune orbit (LPO). This kind of orbit can serve as a platform for transport communication between the lunar surface and the working NRHO. Lunar regions attainable after a one-impulse NRHO departure maneuver are identified, and the costs required for the soft landing are analytically estimated based on the classical gravity-turn landing strategy. In the scenario of a two-impulse transfer to the intermediate LPO, a wide range of perilune distances and inclinations is proved to be available. Several resonant NRHOs have been considered as a working orbit: the 4:1 and 9:2  $L_2$  orbits, and the 11:3  $L_1$  orbit. The calculations are performed in a high-fidelity model of motion that includes the JPL's DE430 ephemeris model of the Solar system and solar radiation pressure. The lunar gravitational field is evaluated based on the GRGM1200A spherical harmonic model truncated to degree and order 8.

## I. INTRODUCTION

Near-rectilinear halo orbits (NRHOs) are a type of periodic orbits that belong to the families of halo orbits around the  $L_1/L_2$  points in a three-body system and have low minimum distances to the smaller primary. They have been independently discovered for the Earth-Moon system by the Soviet researcher M. Lidov [1] and J. Breakwell and J. Brown [2] at the end of the 1970s. The distinct feature of NRHOs is their mild instability or even marginal stability. In the  $L_1$  family of lunar halo orbits, there is only one interval of stable orbits, whereas in the  $L_2$  family, two stability intervals exist (Fig. 1). Those NRHOs which are in resonance with the lunar synodic cycle (about 29.53 days) are of special interest because of simpler shadow avoidance and better predictability of orbital operations due to the periodic behavior of the Earth-Moon-spacecraft mutual configuration.

In recent time, the favorable features of NRHOs attracted the attention of researchers in connection with the problem of choosing an orbit for the near-future crewed lunar orbital station [3,4]. Currently,

the 9:2 NRHO is considered nominal in the ongoing project called the Lunar Orbital Platform-Gateway (LOP-G, previously known as the Deep Space Gateway) [5]. Various aspects of operating the lunar station in a resonant NRHO have been deeply studied, including station-keeping techniques, Earth-NRHO and NRHO-Earth transfer opportunities, challenges in short-term and long-term navigation, eclipse conditions, and shadow avoidance strategies [4,6,7].

In the meantime, few publications have yet been devoted to the problem of lunar landing for a spacecraft in a libration point orbit. Ulybyshev [8] solved this problem numerically, by reducing it to the high-dimensional linear programming problem; however, he considered only halo orbits of small out-of-plane amplitude. Moreover, the approaching trajectory is supposed to have a perilune above the lunar surface, which is generally not necessary. Little information is also available about low-perilune orbits accessible from halo orbits and, particularly, NRHOs. As was concluded in Sec. 3.5.1 of the monograph by Parker and Anderson [9], almost any perilune distance and inclination values can be targeted by naturally (i.e.,

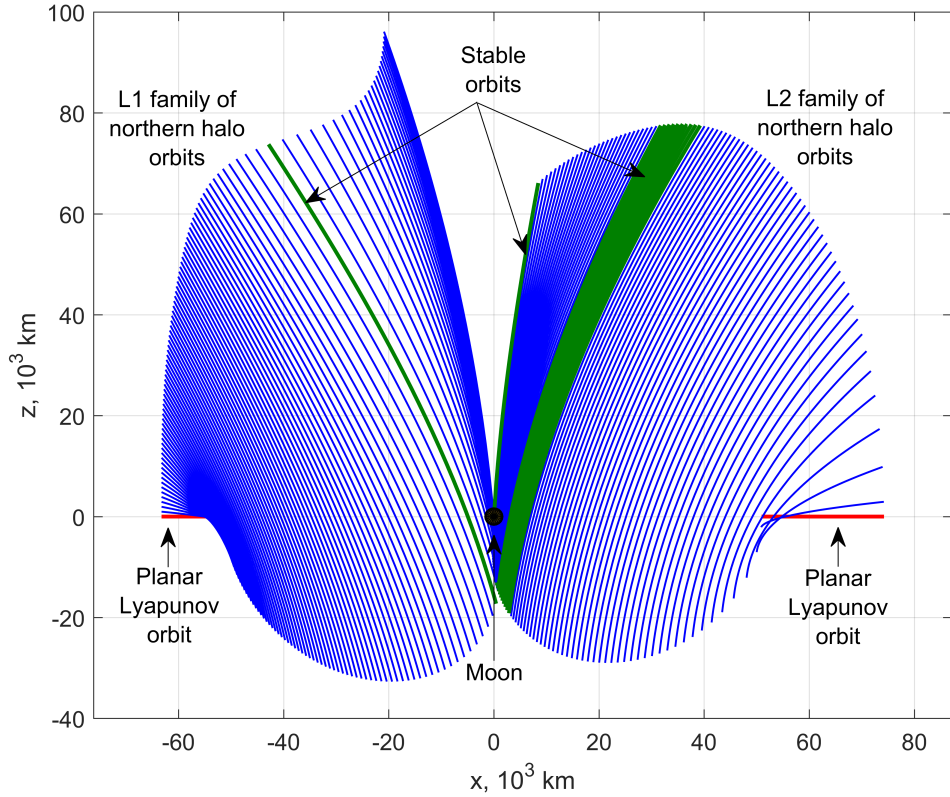


Fig. 1: The lateral ( $xz$ ) view of northern halo orbits around the lunar  $L_1$  and  $L_2$  points.

along the unstable manifold) departing from one of halo orbits in the  $L_2$  family. However, NHROs are just mildly unstable or even stable, and another approach is required to get to a low-perilune orbit (for example, to apply a considerable departure impulse or include a low-thrust arc).

In the current study, we fill the existing gap by considering the problem of transferring a lunar lander from the working resonant NRHO to either the Moon's surface (the scenario of direct landing with a near-parabolic approaching velocity) or some low-perilune orbit. In the former case, the parameters of the descent are estimated by the famous analytical relations derived for the gravity-turn technique. In the latter case, the accompanying problem of a low-perilune orbit stabilization is also solved taking into account the irregular lunar gravity field. The structure of the paper is as follows. In Sec. II, we outline the dynamical models used and the basic properties of NRHOs. The gravity-turn landing fundamentals are recalled in Sec. III. Finally, the results obtained in a high-fidelity model of motion for three resonant NRHOs (11:3  $L_1$ , 4:1  $L_2$ , and 9:2  $L_2$ ) are presented in Sec. IV. All the conclusions made are collected in the corresponding section.

## II. GEOMETRY AND DYNAMIC PROPERTIES OF NEAR-RECTILINEAR HALO ORBITS

### II.I Circular restricted three-body problem

Two dynamical models are used throughout the analysis: the circular restricted three-body problem (CR3BP) and the high-fidelity ephemeris model. To start with, let us introduce the traditional notation for the CR3BP model.

According to the CR3BP model, two masses  $m_1$  and  $m_2$  (without loss of generality,  $m_2 \leq m_1$ ) move in circular orbits about their barycenter  $C$ , and the spacecraft or station of negligible mass moves in the gravitational field of  $m_1$  and  $m_2$ . The equations of motion are usually written in the standard rotating coordinate frame (Fig. 2) with the origin at  $C$ . The  $x$ -axis connects the masses  $m_1$  and  $m_2$  towards  $m_2$ , the  $z$ -axis is directed along the orbital angular momentum of  $m_2$  around  $m_1$ , and the  $y$ -axis completes the right-handed system.

It is convenient to use a dimensionless system of units in which 1) the masses are normalized so that  $m_1 = 1 - \mu$  and  $m_2 = \mu$  where  $\mu = m_2/(m_1 + m_2)$  is the mass parameter of the system, 2) the angular

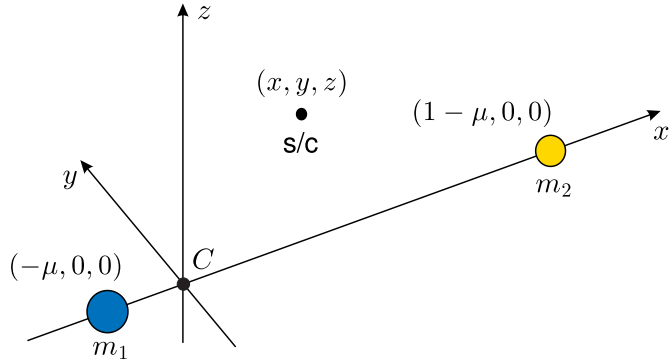


Fig. 2: Rotating frame in the circular restricted three-body problem.

velocity of the rotating frame is normalized to one, as well as the distance between  $m_1$  and  $m_2$ . In this case,  $m_1$  and  $m_2$  are at fixed positions  $(-\mu, 0, 0)$  and  $(1 - \mu, 0, 0)$  on the  $x$ -axis. The equations of motion are expressed in the nondimensional form as

$$\begin{aligned}\ddot{x} - 2\dot{y} &= U_x \\ \ddot{y} + 2\dot{x} &= U_y \\ \ddot{z} &= U_z\end{aligned}\quad [1]$$

where

$$U(x, y, z) = \frac{x^2 + y^2}{2} + \frac{1 - \mu}{r_1} + \frac{\mu}{r_2}$$

is the effective potential and  $U_x$ ,  $U_y$  and  $U_z$  are the partial derivatives of  $U$  with respect to the position variables. The distances to  $m_1$  and  $m_2$  are given by the equalities

$$\begin{aligned}r_1^2 &= (x + \mu)^2 + y^2 + z^2 \\ r_2^2 &= (x - 1 + \mu)^2 + y^2 + z^2\end{aligned}$$

The system (1) has five equilibrium points called libration or Lagrangian points. Three of them lying on the  $x$ -axis, are named collinear. Usually denoted by  $L_1$ ,  $L_2$ , and  $L_3$ , these points are proved to be unstable. Of most interest are the  $L_1$  and  $L_2$  points in the Earth-Moon system. Their  $x$ -coordinates are:

$$\begin{aligned}x_{L1} &= 0.836915131427382 \\ x_{L2} &= 1.155682161024677\end{aligned}$$

In the Earth-Moon system, the mass parameter is taken below as  $\mu = 0.012150584460351$ . The units of distance, velocity, and time are then as follows:

$$\begin{aligned}DU &= 384405 \text{ km} \\ VU &= 1.018296788017434 \text{ km/s} \\ TU &= 4.369189804778479 \text{ days}\end{aligned}$$

## II.II Geometry of near-rectilinear halo orbits

Halo orbits are three-dimensional periodic orbits orthogonal to the  $xz$ -plane of the rotating reference frame. The lateral ( $xz$ ) view of the lunar  $L_1$  and  $L_2$  northern families of halo orbits was already shown in Fig. 1. The frontal ( $yz$ ) view of some typical halo orbit is demonstrated in Fig. 3. The southern families are symmetric to the northern ones with respect to the  $xy$ -plane.

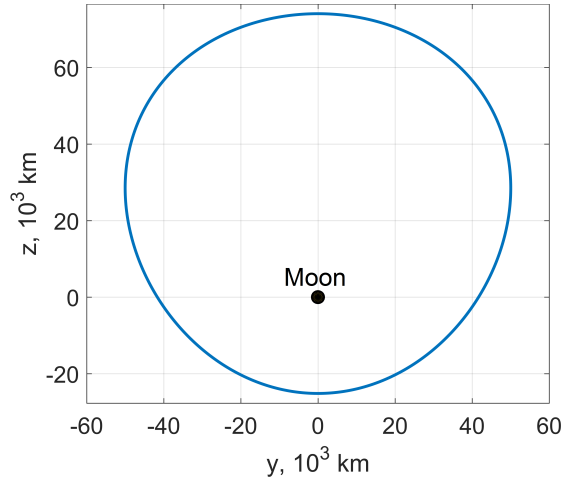


Fig. 3: The frontal view (as seen from the Earth) of a sample lunar  $L_2$  halo orbit.

Halo orbits, though being libration point orbits, do not exist in the close vicinity of a collinear libration point. They branch from planar periodic orbits (also known as planar Lyapunov orbits) at the specific energy level depending on  $\mu$ . As we move along any halo orbit family, the minimum distance to the smaller primary decreases. All the families end with collision orbits. A portion of orbits coming closer to the smaller primary than a certain limit are named

near-rectilinear halo orbits. In the Earth-Moon system, this limit is conventionally set as about 20,000 km. The behavior of the orbital period as a function of the perilune distance for the whole set of NRHOs is depicted in Fig. 4.

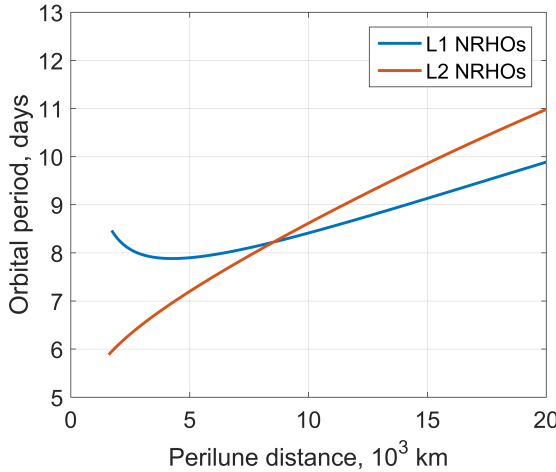


Fig. 4: The perilune distance and the orbital period of the lunar  $L_1$  and  $L_2$  NRHOs.

### II.III Stability of near-rectilinear halo orbits

It is interesting to note that some of the NRHOs are marginally stable in the CR3BP model; station-keeping impulses are so small that some of them can be skipped.

The Floquet theory states that local stability of a periodic orbit is determined by the eigenvalues of the corresponding monodromy matrix. Specifically, if all the eigenvalues lie within the unit circle on the complex plane, the orbit is locally stable; otherwise, it is unstable. To calculate the monodromy matrix associated with the point  $\xi_0 = (x_0, y_0, z_0, \dot{x}_0, \dot{y}_0, \dot{z}_0)$  of the periodic orbit  $\xi(t)$  with  $\xi(t_0) = \xi_0$ , one needs to solve the variational equations

$$\dot{\Phi}(t; t_0) = \mathbf{A}(t)\Phi(t; t_0) \quad [2]$$

with the initial condition  $\Phi(t_0; t_0) = \mathbf{I}_{6 \times 6}$  (the  $6 \times 6$  identity matrix). The matrix  $\mathbf{A}(t)$  in Eq. (2) is the Jacobian of the function  $\mathbf{f}(\xi)$  in the right-hand side of the initial dynamical system for  $\xi$  evaluated along the orbit  $\xi(t)$ . For the CR3BP model, it is seen from Eq. (1) that

$$\mathbf{f}(\xi) = \begin{pmatrix} \dot{x} \\ \dot{y} \\ \dot{z} \\ 2\dot{y} + U_x \\ -2\dot{x} + U_y \\ U_z \end{pmatrix}$$

$$\mathbf{A}(t) = \begin{pmatrix} 0 & 0 & 0 & 1 & 0 & 0 \\ 0 & 0 & 0 & 0 & 1 & 0 \\ 0 & 0 & 0 & 0 & 0 & 1 \\ U_{xx} & U_{xy} & U_{xz} & 0 & 2 & 0 \\ U_{xy} & U_{yy} & U_{yz} & -2 & 0 & 0 \\ U_{xz} & U_{yz} & U_{zz} & 0 & 0 & 0 \end{pmatrix} \xi = \xi(t)$$

When integrating Eq. (2) over the orbital period  $P$ , one computes the monodromy matrix  $\Phi(t_0 + P; t_0)$ . Its eigenvalues do not depend on the reference point  $\xi_0$  and, therefore, serve as the characteristics of the orbit.

For halo orbits with a small enough  $z$ -amplitude, the monodromy matrix has 6 eigenvalues

$$\lambda_1 > 1, \lambda_2 = \lambda_1^{-1} < 1, \lambda_3 = \lambda_4 = 1$$

$$\lambda_5 = \lambda_6^*, |\lambda_5| = |\lambda_6| = 1$$

where  $\lambda_5$  and  $\lambda_6$  are complex conjugates. When we move along the family, the eigenvalues start shifting on the complex plane so that  $\lambda_1 \rightarrow 1, \lambda_2 \rightarrow 1$ , while the other eigenvalues drift along the unit circle. At some moment, all the eigenvalues appear to migrate onto the unit circle, and the periodic orbit becomes marginally stable (in the linear sense). The region of stability ends when one of the eigenvalues migrates outside the unit circle. As it was said earlier, among the lunar  $L_2$  NRHOs, there are two intervals of stable orbits, whereas among the  $L_1$  NRHOs, a single stability interval exists (Figs. 5–6).

It is worth emphasizing that a periodic orbit can lose the property of marginal stability when perturbations are added. So, the analysis in the ephemeris model is required.

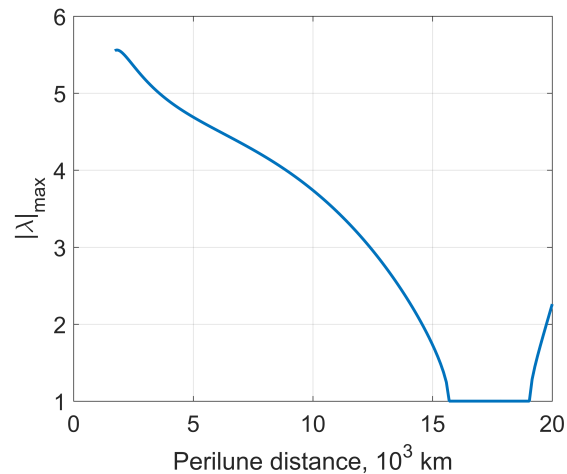


Fig. 5: Variation of the largest eigenvalue modulus with the perilune distance for the  $L_1$  NRHOs.

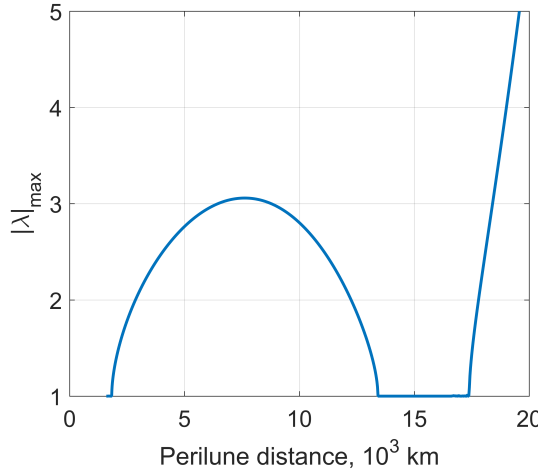


Fig. 6: Variation of the largest eigenvalue modulus with the perilune distance for the  $L_2$  NRHOs.

#### II.IV High-fidelity model of orbital motion

In addition to the CR3BP model, the ephemeris model of motion is used for high-accuracy modeling. Positions of the Sun and the Solar system's planets, as well as the instantaneous orientation of the lunar principal axes of inertia relative to the International Celestial Reference System (ICRS) coordinate axes, are retrieved from JPL's DE430 ephemeris [10]. For solar radiation pressure, the cannonball model with the area-to-mass ratio  $A/m = 0.006 \text{ m}^2/\text{kg}$  is used. The lunar gravitational acceleration  $\mathbf{g}_m$  is evaluated based on the spherical harmonic model truncated to

degree and order 8 [11]. The equations of spacecraft motion are written in the following form:

$$\ddot{\mathbf{r}} = \mathbf{g}_m - \frac{PA}{m} \frac{\mathbf{r}_s - \mathbf{r}}{|\mathbf{r}_s - \mathbf{r}|} + \frac{\mu_s}{|\mathbf{r}_s - \mathbf{r}|^3} (\mathbf{r}_s - \mathbf{r}) - \frac{\mu_s}{|\mathbf{r}_s|^3} \mathbf{r}_s + \sum_{i=1}^8 \left( \frac{\mu_i}{|\mathbf{r}_i - \mathbf{r}|^3} (\mathbf{r}_i - \mathbf{r}) - \frac{\mu_i}{|\mathbf{r}_i|^3} \mathbf{r}_i \right)$$

The indices  $m$ ,  $s$ , and  $i$  relate to the Moon, the Sun, and the  $i$ -th planet, respectively. All the vectors are expressed in the Moon-centered inertial system with the axes parallel to the ICRS axes. Such a system is called the Selenocentric Celestial Reference System (SCRS). The gravitational parameters  $\mu_i$ ,  $i = 1 \dots 8$ , and  $\mu_s$  have been taken from the 2018 Astronomical Almanach.\* The constant value  $P = 4.56 \cdot 10^{-6} \text{ Pa}$  of solar radiation pressure was adopted in modeling. When indicating points on the lunar surface, we use their selenographic latitude and longitude in the so-called Mean-Earth/Mean-Rotation System (MER). The transformation from the Moon's principal axes of inertia to the MER axes is described, for instance, in [10]. The inclination of low-perilune orbits is also given with respect to the MER equatorial plane.

Among all the NRHOs in synodic resonance, we select only three—9:2  $L_2$ , 4:1  $L_2$ , and 11:3  $L_1$ —that exhibit compact, nearly-periodic motion (see Fig. 7) and have a sufficiently low perilune altitude (about 1500–3000 km). It is these orbits, both northern and southern, that are considered further in the text.

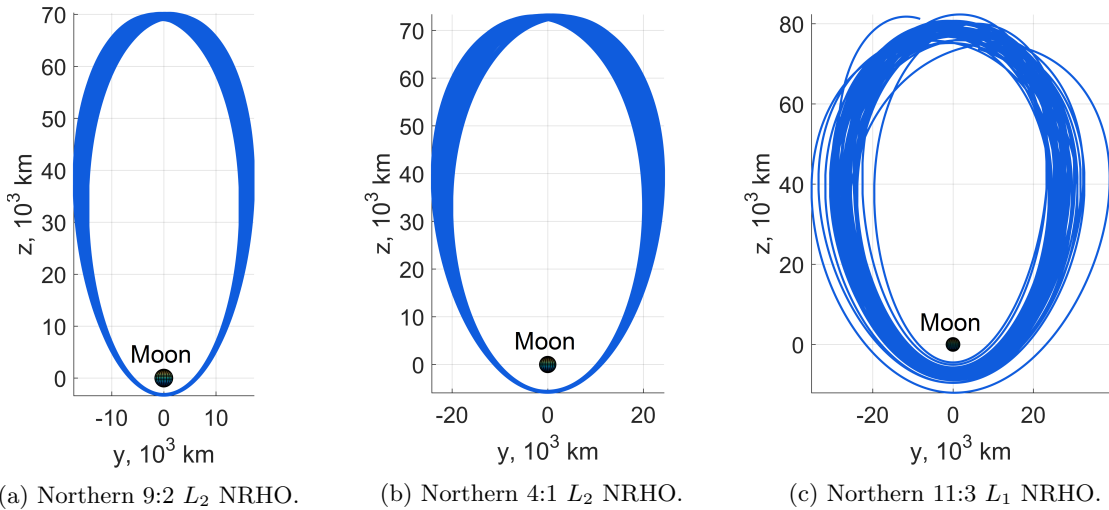


Fig. 7: Selected resonant NRHOs from the  $L_1$  and  $L_2$  northern families adapted to the ephemeris model.

\*See <http://asa.usno.navy.mil/>.

### III. GRAVITY-TURN LANDING TECHNIQUE

#### III.I Brief review of existing landing techniques

During half a century from successful landings of Apollo spacecraft, a lot of lunar landing approaches have been proposed and developed. Early strategies are primarily analytical and non-optimal in terms of fuel consumption. In real lunar missions, two major phases of the landing process are distinguished, the braking phase and the approach phase. The former aims at nullifying the greater portion of the lander's orbital velocity, whereas the latter ensures a vertical orientation of the lander above the landing site. The Apollo descent guidance algorithm implies that the thrust acceleration is expressed as a quadratic function of time, the total descent time being fixed [12]. In this case, a trajectory is represented as a quartic polynomial in time.

Another well-known and flight-proven analytical strategy is the gravity-turn technique [13]. Its main assumption is that the direction of the thrust vector is opposite to the velocity vector at every moment of time. Such a guidance law automatically attains the objectives of the two phases, while being sufficiently close to the propellant-optimal law when the initial altitude is small enough compared to the body's radius. Upon analytically constructing the trajectory of descent, one can use it as a nominal one in closed-loop algorithms of terminal (re)targeting under the complex terrain conditions [14, 15].

The important drawback of the above strategies is the lack of optimality. The heavier the lander, the more critical this issue. Since the descent trajectory arc is usually short (up to 8-10 deg) and confined to the thin spherical layer around a celestial body, the assumption of uniform gravity field is applied in the majority of researches. For such a simple dynamical model, the fuel-optimal control problem appears to be trivial and has been solved by several researchers long before the discovery of Pontryagin's maximum principle (see, e.g., [16]). According to this solution, the thrust (pitch) angle  $\theta$  changes as

$$\tan \theta = \frac{c_1 + c_2 t}{c_3 + c_4 t} \quad [3]$$

where  $c_i$ ,  $i = 1, \dots, 4$ , are some constants. The same bilinear tangent law is proved to be optimal when a pitch constraint is imposed [17]. Eq. (3) degenerates into the linear tangent law ( $c_4 = 0$ ) or the constant thrust attitude law ( $c_2 = c_4 = 0$ ) for a specific set of boundary conditions. The optimal trajectory is not expressed in a closed form, but can be approximated by polynomials and tracked by means of an onboard

controller [18]. To ensure the vertical landing at the terminal descent phase, an additional constraint can be included in the Hamiltonian [19]. Another option is to exploit the optimal solution only at the braking phase [20]<sup>†</sup> and then switch to strategies satisfying the operational constraints, such as the polynomial-based technique used in the Apollo missions. In case of deorbiting from a high-altitude parking orbit, the perilune altitude of the intermediate elliptical orbit can be selected optimally based on the parking orbit altitude and the thrust capacity [21]. The attitude kinematical and dynamical constraints can substantially influence the optimization results and need to be taken account [22].

A renewed interest in studying the powered descent guidance problem is associated with the plans of colonizing Mars and establishing a Martian base. Advanced requirements, such as a pinpoint landing, are hard to meet without using efficient indirect [23] or direct [24, 25] optimization solvers. Increased on-board computational resources alleviate the issue of integrating them in real-flight guidance algorithms.

One of the aims of the present study is to assess the accessible regions of the lunar surface where the direct landing from the selected resonant NRHOs is possible. The gravity-turn strategy, with its simple, explicit formulas relating the design parameters and the performance characteristics, is accurate enough to capture all the principal qualitative patterns. So, it is this landing strategy that we will further use in our estimations.

#### III.II Assumptions and approximations used

The general scheme of the direct landing from an NRHO starts with the impulsive departure maneuver. An impulse applied at some point of the NRHO sends the lander towards the Moon. The perilune of the transfer orbit is low (or even below the surface). We suppose that the gravity-turn maneuver is initiated at some point of the transfer orbit close enough to the Moon. Since the approaching velocity is quite high, the descent trajectory arc can be long, and the circular model of the Moon should be exploited. The magnitudes of the gravitational acceleration  $g_m$  and the retrothrust acceleration  $a_t$  are both supposed to be constant throughout the maneuver. Therefore, it is also true for the thrust-to-weight ratio  $n = a_t/g_m$ .

The approaching trajectory is a fly-by trajectory if the perilune altitude  $h_\pi$  is positive (see Fig. 8), or a collision trajectory when  $h_\pi < 0$ . In any case, this near-Moon part of the transfer orbit is considered to be Keplerian, with the semilatus rectum value  $p$  and

<sup>†</sup>Note that a different functional is minimized in that paper.

the eccentricity  $e$  (can be greater than 1). The point of initiating the gravity-turn maneuver is unknown; it needs to be determined for a given level of thrust. Its altitude is denoted by  $h_0$  and the corresponding flight path angle  $\gamma_0$  is assumed negative.

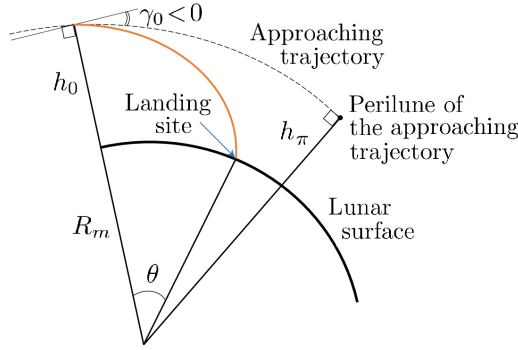


Fig. 8: Principal scheme of the direct landing.

### III.III Analytical relationships for the gravity-turn landing parameters

In the celebrated paper by Citron et al. [13], the analytical relationship is derived that dictates what level of thrust-to-weight ratio ensures soft landing if the gravity-turn maneuver begins at the altitude  $h_0$  where the spacecraft velocity has a magnitude of  $v_0$  and is directed at angle  $\gamma_0 < 0$  to the local horizontal plane. For the circular Moon model, the required thrust-to-weight ratio level is obtained as a positive root of the quadratic equation

$$n^2 + \left( \frac{v_0^2}{2g_m h_0} + 1 \right) n \sin \gamma_0 - \frac{v_0^2 \cos^2 \gamma_0}{4g_m h_0} \times \\ \times \left( 1 + \frac{2g_m h_0}{v_0^2} \right)^2 \left( 1 - \frac{v_0^2}{2g_m R_m} \right) = 0 \quad [4]$$

This equation has only one positive root if  $v_0$  is less than the escape velocity of the Moon  $\sqrt{2g_m R_m}$  [13]. The downrange  $d$  and the central angle  $\theta$  traversed

---


$$n^2 - \sqrt{1 - \frac{1 + \bar{h}_\pi}{1 + \bar{h}_0}} \left[ \frac{1}{\bar{h}_0 (1 + \bar{h}_0)} + 1 \right] n - \frac{1}{2\bar{h}_0 (1 + \bar{h}_0)} \frac{1 + \bar{h}_\pi}{1 + \bar{h}_0} [1 + \bar{h}_0 (1 + \bar{h}_0)]^2 \left( 1 - \frac{1}{1 + \bar{h}_0} \right) = 0$$


---

This formula can be treated as a quadratic equation

$$\frac{\alpha^2}{2} - \sqrt{\bar{h}_0 - \bar{h}_\pi} \alpha - (1 + \bar{h}_\pi) \bar{h}_0^2 = 0$$

with respect to the new variable

$$\alpha = 2n\bar{h}_0 (1 + \bar{h}_0)^{3/2} [1 + \bar{h}_0 (1 + \bar{h}_0)]^{-1}$$

by the spacecraft's radius vector during the gravity-turn maneuver (see Fig. 8) are calculated according to the formula

$$d \equiv \theta R_m = \frac{v_0^2 \cos \gamma_0}{2a_t} \frac{v_0^2 + 2g_m h_0}{v_0^2 + g_m h_0} \frac{R_m}{R_m + h_0} \quad [5]$$

The time of descent

$$T = \frac{v_0}{a_t} \left( 1 + \frac{2g_m h_0}{v_0^2} \right) \quad [6]$$

allows estimating the gravity-turn maneuver cost:

$$\Delta V \equiv a_t \cdot T = v_0 + \frac{2g_m h_0}{v_0} \quad [7]$$

### III.IV Applicability of the gravity-turn technique to the case of a rapidly approaching lander

The above estimates appear to be applicable not only to the problem of soft landing from a low lunar orbit with  $\gamma_0 \approx 0$  but also to landing from a collision or fly-by approaching trajectory. The eccentricity of such a trajectory can be very close to or even exceed one. To the best of our knowledge, the applicability conditions for the gravity-turn strategy have not yet been stated explicitly in this case. Meanwhile, as we will further see, after the departure from an NRHO, all the approaching trajectories have an eccentricity  $e \simeq 1$ .

Let us consider a parabolic ( $e = 1$ ) approaching trajectory and derive the applicability condition for Eqs. (4-7). Upon introducing the notation

$$\bar{h}_0 = \frac{h_0}{R_m}, \quad \bar{h}_\pi = \frac{h_\pi}{R_m}$$

and recalling that

$$\cos^2 \gamma = \frac{\mu_m p}{r^2 v^2} = \frac{p}{2r} = \frac{r_\pi}{r}$$

in any point of a parabolic trajectory, we can rewrite Eq. (4) as

---


$$n^2 - \sqrt{1 - \frac{1 + \bar{h}_\pi}{1 + \bar{h}_0}} \left[ \frac{1}{\bar{h}_0 (1 + \bar{h}_0)} + 1 \right] n - \frac{1}{2\bar{h}_0 (1 + \bar{h}_0)} \frac{1 + \bar{h}_\pi}{1 + \bar{h}_0} [1 + \bar{h}_0 (1 + \bar{h}_0)]^2 \left( 1 - \frac{1}{1 + \bar{h}_0} \right) = 0$$


---

The only positive root is given by the expression

$$\alpha = \sqrt{\bar{h}_0 - \bar{h}_\pi} + \sqrt{\bar{h}_0 - \bar{h}_\pi + 2(1 + \bar{h}_\pi) \bar{h}_0^2}$$

Taking into account that  $\bar{h}_0 \ll 1$ , we obtain

$$\bar{h}_\pi \approx \bar{h}_0 - \frac{\alpha^2}{4} \approx \bar{h}_0 - n^2 \bar{h}_0^2$$

The nondimensional perilune altitude  $\bar{h}_\pi$  for the approaching trajectory is not allowed to take a value greater than

$$\bar{h}_\pi^{\max} = \frac{1}{4n^2} \quad [8]$$

in order the nondimensional altitude  $\bar{h}_0$  of the point where the gravity-turn maneuver begins be positive real. For any  $\bar{h}_\pi \in [-1, \bar{h}_\pi^{\max}]$ , the required value of  $\bar{h}_0$  can be estimated by the formula

$$\bar{h}_0 = \frac{1}{2n^2} + \sqrt{\frac{1}{4n^4} - \frac{\bar{h}_\pi}{n^2}} \quad [9]$$

#### IV. TRANSFERS FROM NEAR-RECTILINEAR HALO ORBITS TO THE MOON

##### IV.I General scheme of the NRHO-Moon transfer

Two scenarios of delivering a lander to the Moon are considered: the direct landing from the working NRHO orbit and the transfer to some intermediate low-perilune orbit (LPO). Six resonant NRHOs are tested in the role of a working orbit: 9:2  $L_2$ , 4:1  $L_2$ , and 11:3  $L_1$ , either northern or southern. The initial phase of the both scenarios is the departure impulse at some point of the working orbit. We examine 100 candidate points that are equally distributed across the period of a given NRHO. The magnitude of the impulse was selected from the following discrete set: 50, 100, ..., 450, 500 m/s. It is worth noting that, in contrast to more unstable libration point orbits, the departure from stable or almost stable NRHOs cannot be executed by applying a negligible burn along the unstable manifold direction. Finally, 92 impulse directions are sampled nearly uniformly on the unit sphere, which gives a set of 92,000 departing trajectories. They are propagated in the ephemeris model. The fixed start date of 1st January 2028 was chosen for all the trajectories.

Most of the 92,000 departing trajectories do not traverse close enough to the Moon and are therefore discarded. So, only 5-10% of the trajectories with a perilune altitude of 300 km or less can be referred to as approaching trajectories. For the northern 9:2  $L_2$  NRHO, Fig. 9 shows the distribution of along-track and radial components of the lander velocity at the 300 km altitude. The velocity magnitude is approximately the same for all the approaching trajectories and is about the local escape velocity

$$v_{\text{esc}} = \sqrt{\frac{2\mu_m}{R_m + 300 \text{ km}}} \approx 2.19 \text{ km/s}$$

It is now clear that the approaching trajectories are almost parabolic, with an eccentricity close to one.

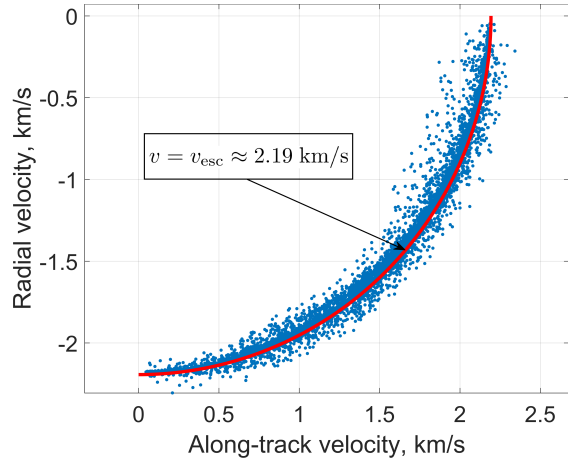


Fig. 9: Velocity components (along-track and radial) at the 300 km altitude. The red arc indicates the local escape velocity.

For a typical thrust-to-weight ratio  $n = 5$ , which corresponds to  $a_t \approx 8 \text{ m/s}^2$ , the maximum perilune altitude  $h_\pi$  when the gravity-turn formulas are still applicable is about 15-17 km, as we see from Eq. (8). On the contrary, for safety reasons, the perilune altitude of an intermediate low-perilune orbit must be greater than that threshold. So, the whole database of approaching trajectories turns out to be naturally separated into two parts, depending on the scenario chosen.

It is interesting to note that a wide interval of inclinations is accessible after applying the departure impulse (see Figs. 10–15). The closer the departure point to the NRHO ascending/descending node, the wider the interval of accessible inclinations. The opposite picture is observed if the departure impulse is applied near the NRHO apolune or perilune. In this case, only polar and near-polar orbits are accessible. At the same time, it is this kind of lunar orbits that is often required in real missions. The lander can be delivered into such orbits with the least cost (within 50-100 m/s) by performing the departure maneuver far enough from the Moon.

One can conclude from Figs. 10–15 that the features described above are qualitatively the same for all the six NRHOs considered.

##### IV.II Direct landing scenario

For the approaching trajectories with a perilune altitude less than 17 km, Eqs. (4-7) can be exploited for estimating the principal landing parameters and performance characteristics, including possible sites of soft landing. These data are compactly visualized in Figs. 16–18.

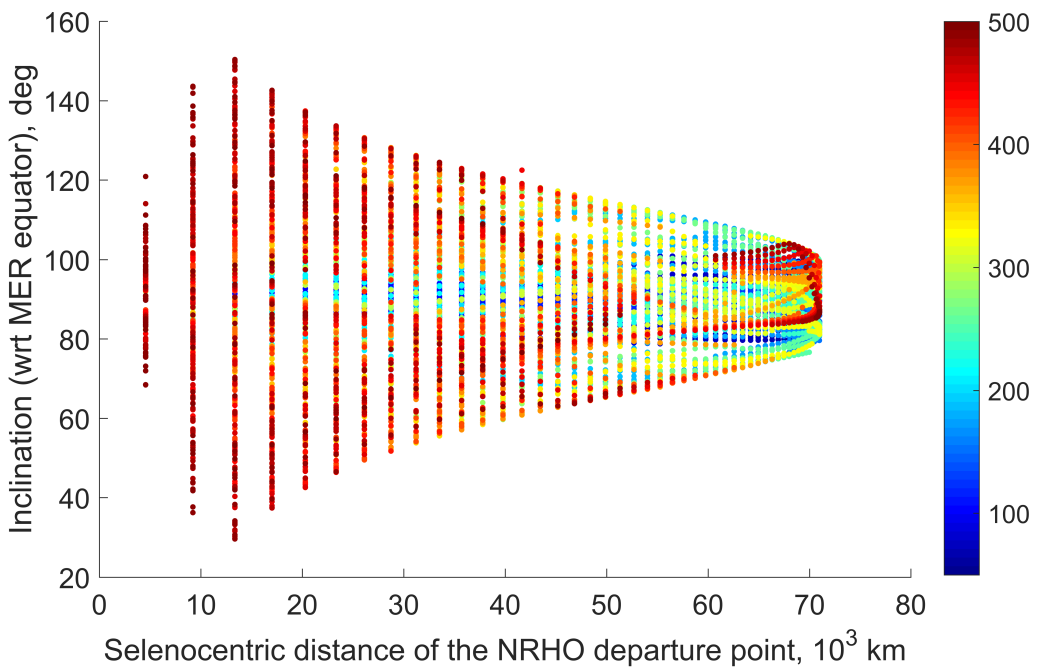


Fig. 10: Inclinations accessible from the northern 9:2  $L_2$  NRHO and the associated departure  $\Delta V$  (in m/s).

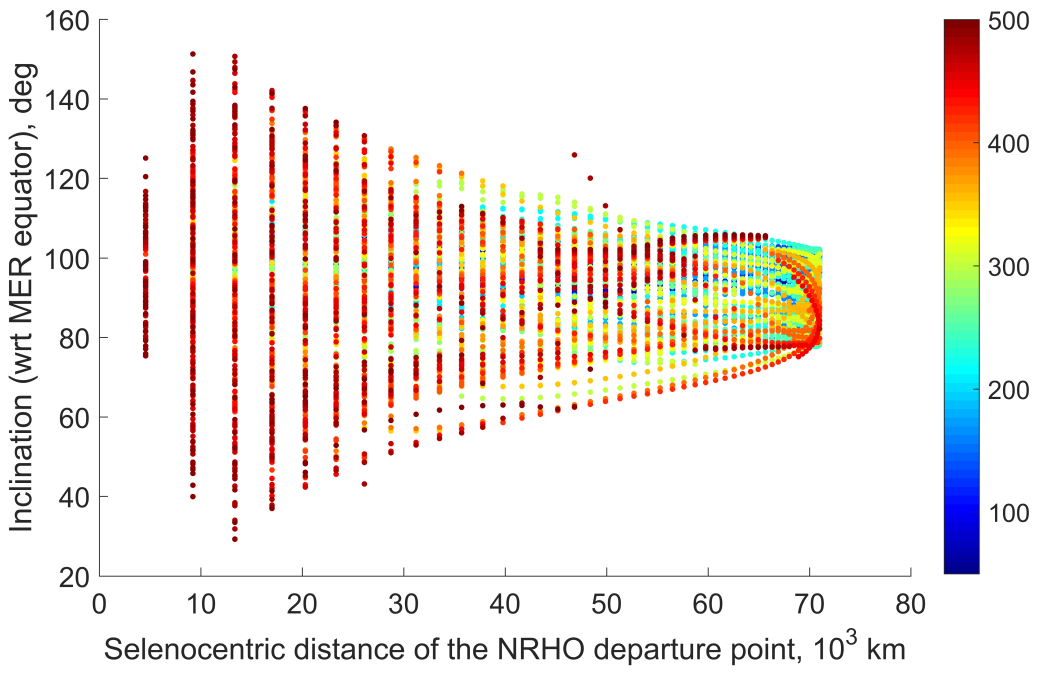


Fig. 11: Inclinations accessible from the southern 9:2  $L_2$  NRHO and the associated departure  $\Delta V$  (in m/s).

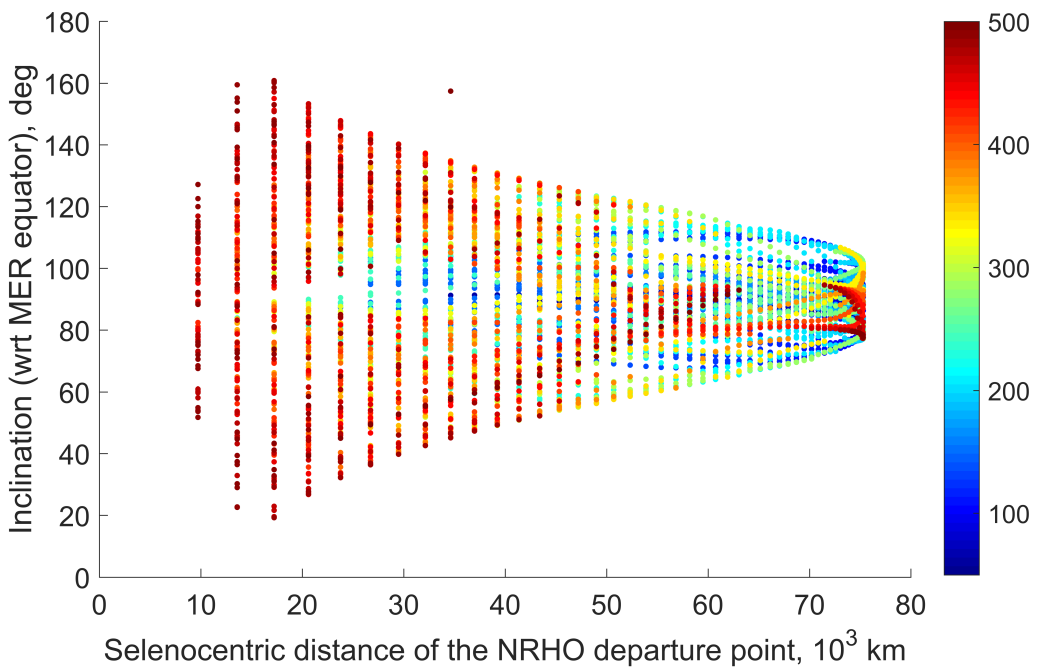


Fig. 12: Inclinations accessible from the northern 4:1  $L_2$  NRHO and the associated departure  $\Delta V$  (in m/s).

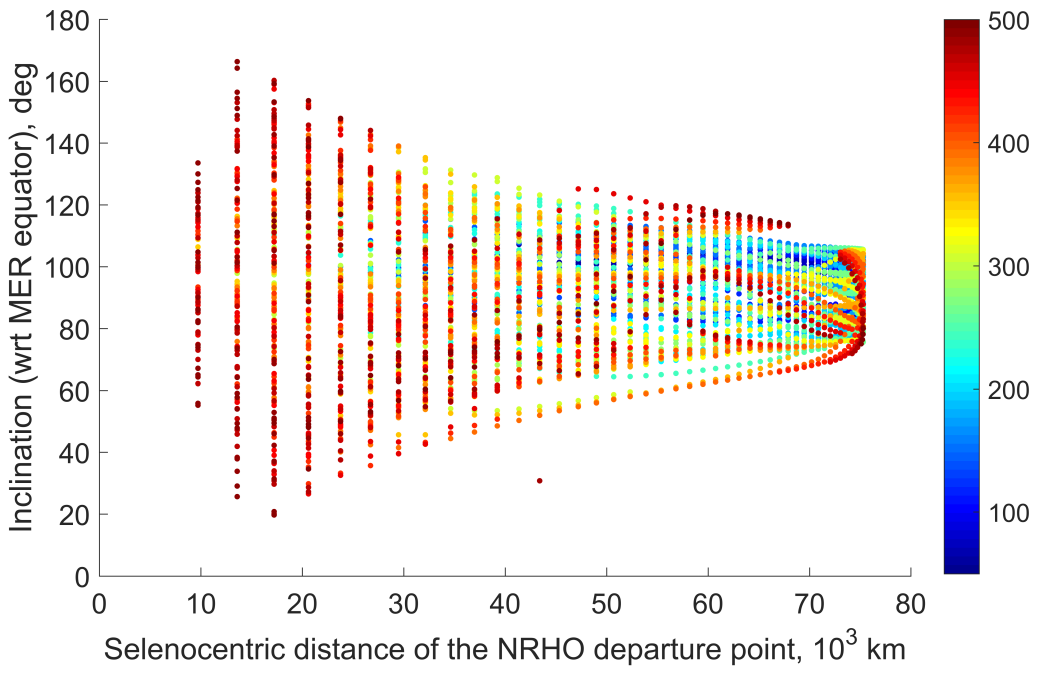


Fig. 13: Inclinations accessible from the southern 4:1  $L_2$  NRHO and the associated departure  $\Delta V$  (in m/s).

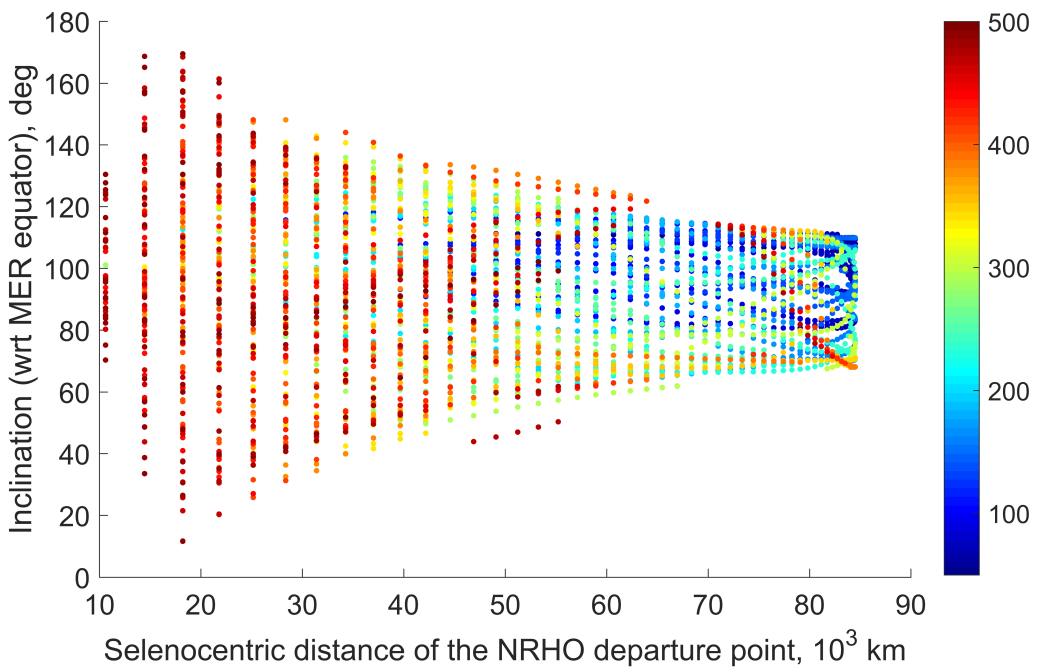


Fig. 14: Inclinations accessible from the northern 11:3  $L_1$  NRHO and the associated departure  $\Delta V$  (in m/s).

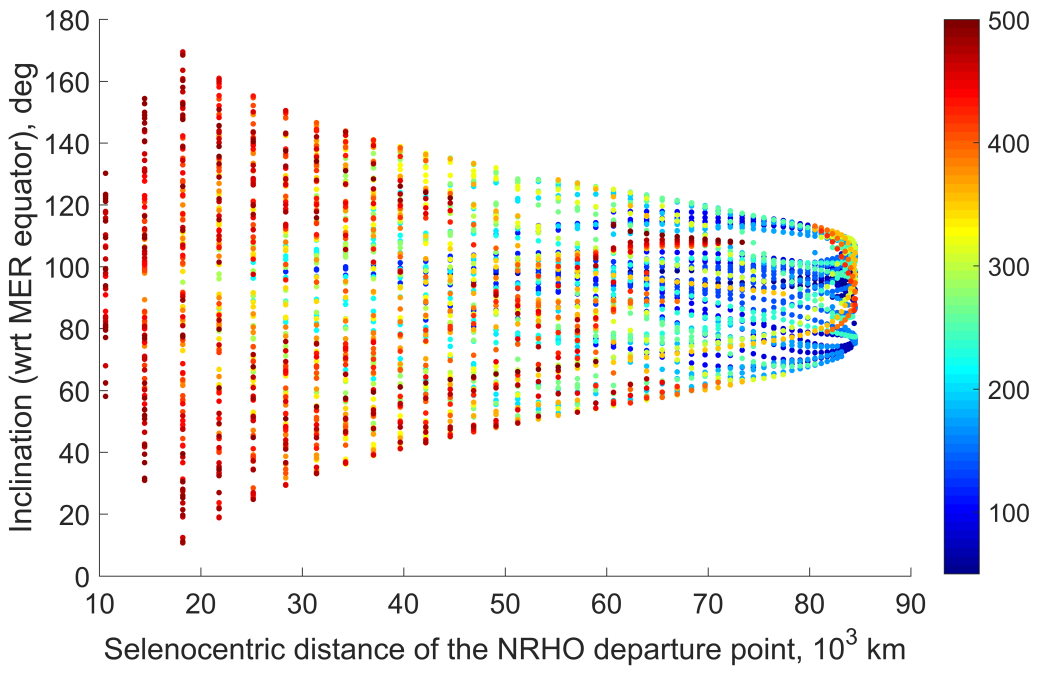
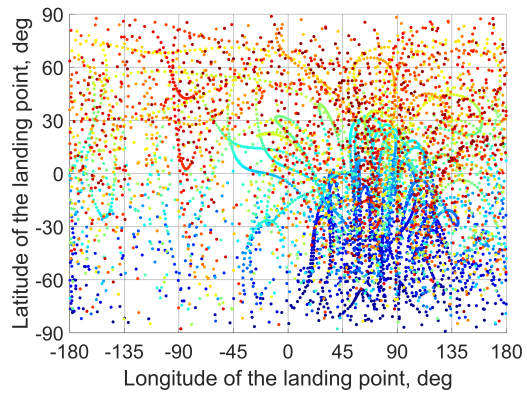
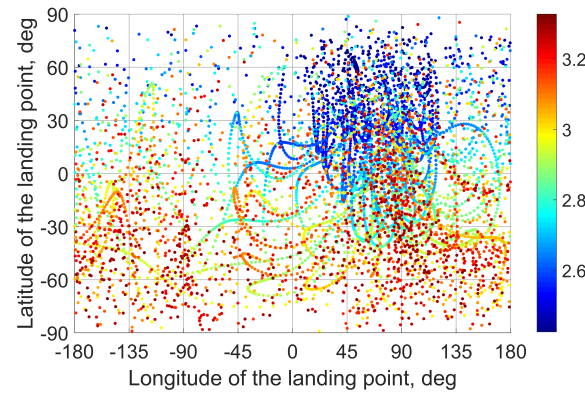


Fig. 15: Inclinations accessible from the southern 11:3  $L_1$  NRHO and the associated departure  $\Delta V$  (in m/s).

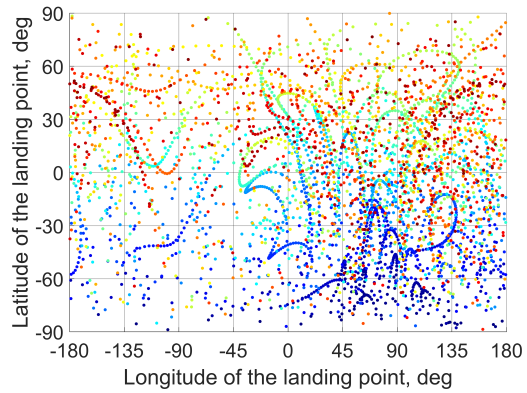


(a) Northern 9:2  $L_2$  NRHO

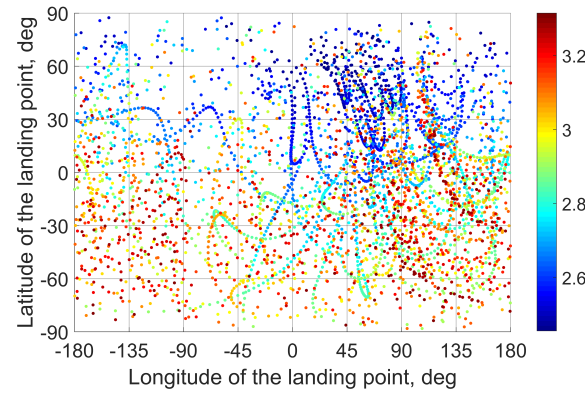


(b) Southern 9:2  $L_2$  NRHO

Fig. 16: Possible sites of direct landing from the 9:2  $L_2$  NRHO and the associated total  $\Delta V$  (in km/s).

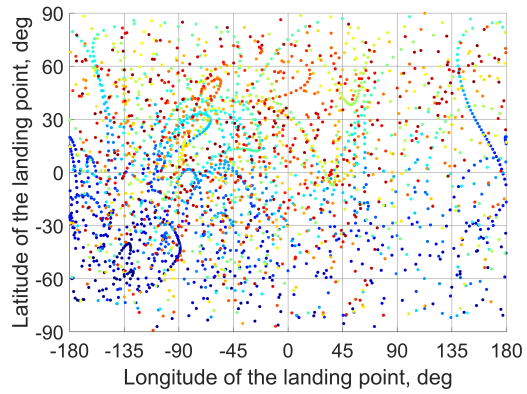


(a) Northern 4:1  $L_2$  NRHO

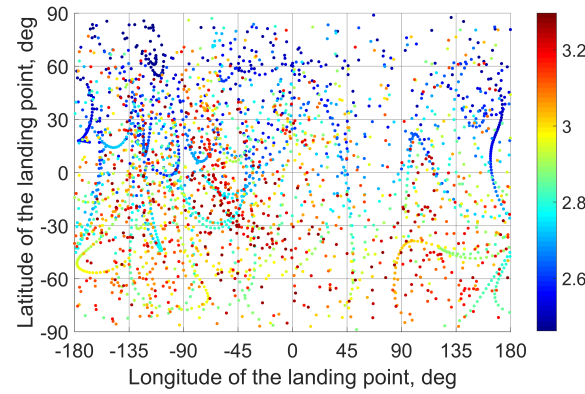


(b) Southern 4:1  $L_2$  NRHO

Fig. 17: Possible sites of direct landing from the 4:1  $L_2$  NRHO and the associated total  $\Delta V$  (in km/s).



(a) Northern 11:3  $L_1$  NRHO



(b) Southern 11:3  $L_1$  NRHO

Fig. 18: Possible sites of direct landing from the 11:3  $L_1$  NRHO and the associated total  $\Delta V$  (in km/s).

Some important observations can be made with regard to reachability of lunar surface regions. First, the whole lunar surface is theoretically available for soft landing from any of the six NRHOs considered. However, optimal landing regions exist for every orbit. For northern NRHOs, minimum- $\Delta V$  departure maneuvers are mostly located along the descending arc (between the apolune and the descending node) of the orbit. Consequently, geometrically convenient landing sites are placed in the southern hemisphere. The opposite situation is true for southern NRHOs. Furthermore, the east-west asymmetry exists for  $L_1$  and  $L_2$  orbits since the direction of approaching the Moon from an  $L_1$  orbit naturally suggests landing in the Moon's western hemisphere, whereas its eastern hemisphere is preferable for landing from  $L_2$  orbits.

Typical values of all the landing parameters are found to be similar for the six NRHOs. For instance, the downrange spans up to 350 km while the time of descent constitutes about 5-6 minutes (Fig. 19). The altitude of initiating the descent burn behaves close to what Eq. (9) predicts for a parabolic approaching trajectory (see Fig. 20).

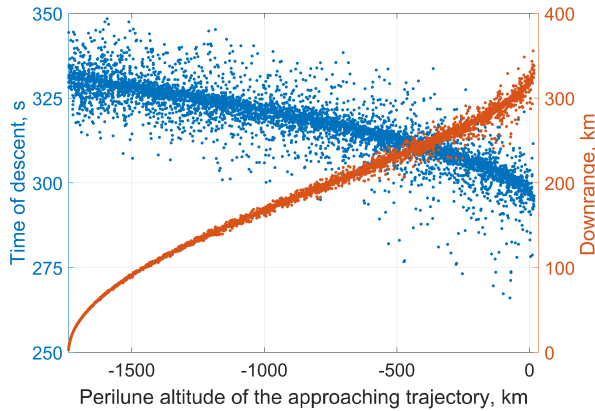


Fig. 19: Time of descent and downrange values for landing from the southern 9:2  $L_2$  NRHO.

#### IV.III Targeting and stabilizing low-perilune orbits

In another scenario, involving a transfer to some low-perilune orbit, the minimum stabilizing impulse at the perilune of approaching trajectories is sought. Upon applying the braking impulse, an approaching trajectory should be transformed in a stable elliptic orbit. By ‘stable’ we imply the orbit whose perilune altitude and inclination variations throughout three consecutive revolutions around the Moon do not exceed 10% and 0.1 deg, respectively.

In Figs. 21–26, the main parameters of stabilized low-perilune lunar orbits—the perilune altitude and

the inclination—are displayed. The color, as before, indicates the total  $\Delta V$  budget for the departure and stabilizing impulses. One can notice the remarkable, eye-catching feature of all the six figures: the almost total absence of any stabilized orbits with a perilune altitude less than 100 km. It results from the highly irregular lunar gravity field that does not allow one-impulse stabilization of approaching trajectories.

What concerns the successfully stabilized orbits, the distribution of the total cost across the range of accessible inclinations is similar to one observed for the departure impulse in Figs. 10–15. The polar and near-polar orbits are again the most affordable.

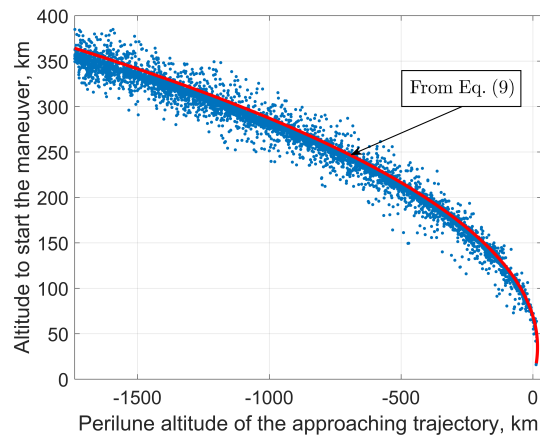


Fig. 20: Altitude of initiating the gravity-turn maneuver for approaching trajectories with different  $\bar{h}_\pi$  (the southern 9:2  $L_2$  NRHO).

#### V. CONCLUSIONS

In this study, the problem of delivering a lander from the working near-rectilinear halo orbit around the Moon directly to the lunar surface (soft landing) or to some intermediate low-perilune orbit has been examined. It was shown that, although any landing site is in principle feasible, there exist areas of least-cost landing. The distribution of these areas across the lunar surface is markedly asymmetric regarding both northern/southern and western/eastern hemispheres. The former asymmetry has appeared to be related to the NRHO subtype (northern/southern), while the latter is connected to what libration point is considered. The landing characteristics have been estimated using the relationships of the gravity-turn landing strategy. Among low-perilune orbits, a wide range of inclinations is accessible, with (near-)polar orbits being stabilizable at lowest cost. The perilune of stabilizable orbits cannot be too low to avoid the influence of the highly irregular lunar gravity field.

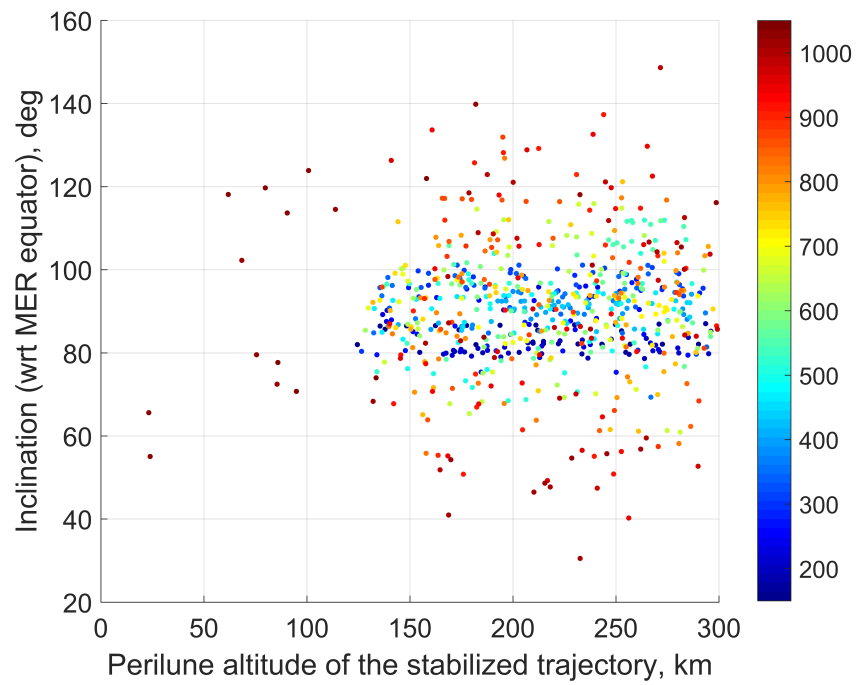


Fig. 21: Inclination and perilune altitude of stable low-perilune orbits accessible from the northern 9:2  $L_2$  NRHO and the associated total  $\Delta V$  (in m/s).

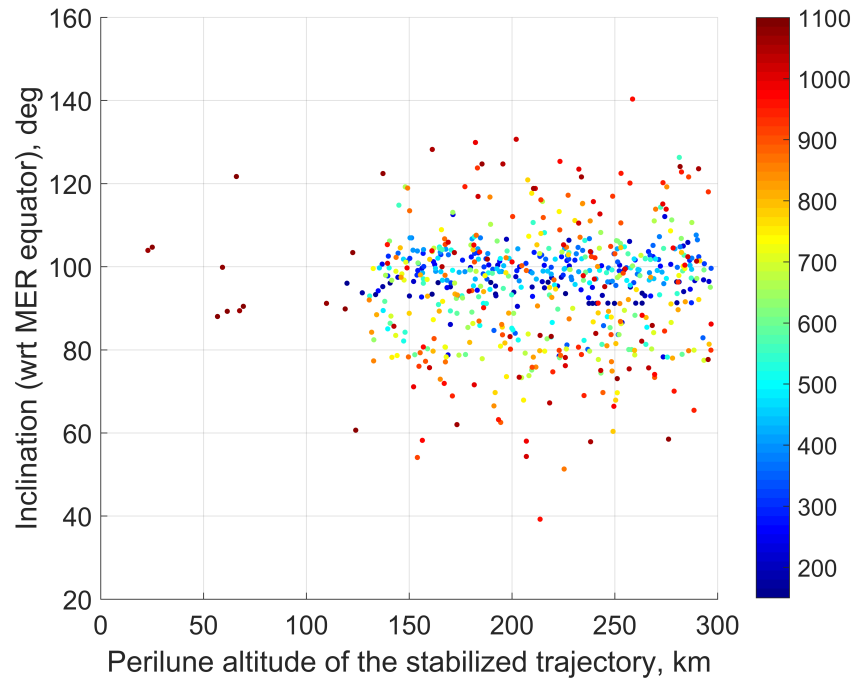


Fig. 22: Inclination and perilune altitude of stable low-perilune orbits accessible from the southern 9:2  $L_2$  NRHO and the associated total  $\Delta V$  (in m/s).

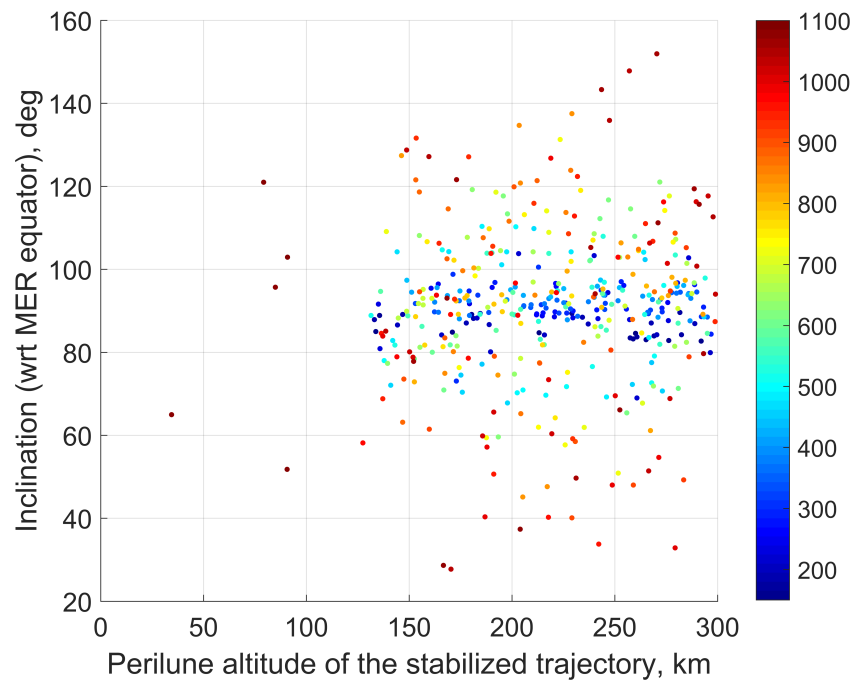


Fig. 23: Inclination and perilune altitude of stable low-perilune orbits accessible from the northern 4:1  $L_2$  NRHO and the associated total  $\Delta V$  (in m/s).

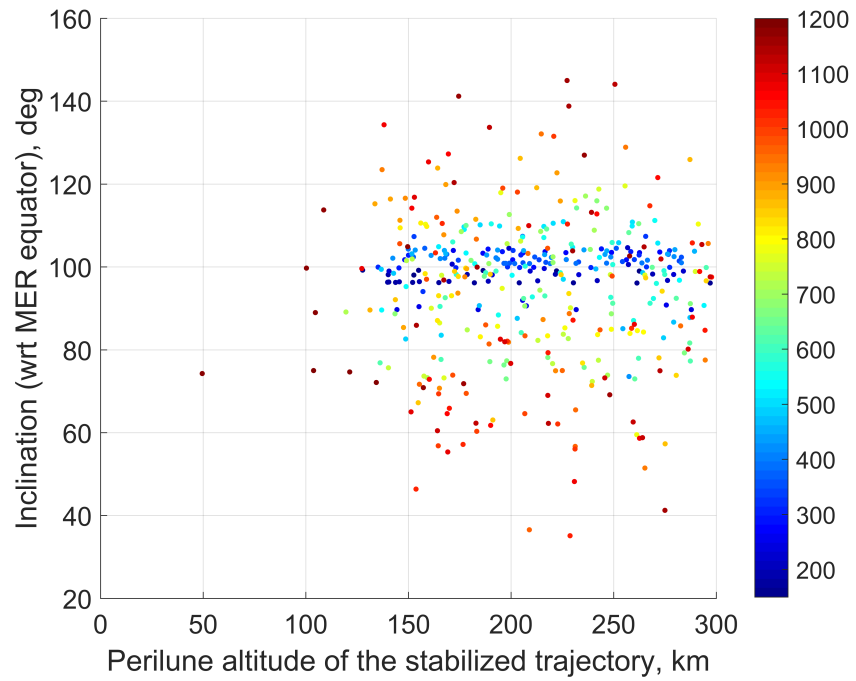


Fig. 24: Inclination and perilune altitude of stable low-perilune orbits accessible from the southern 4:1  $L_2$  NRHO and the associated total  $\Delta V$  (in m/s).

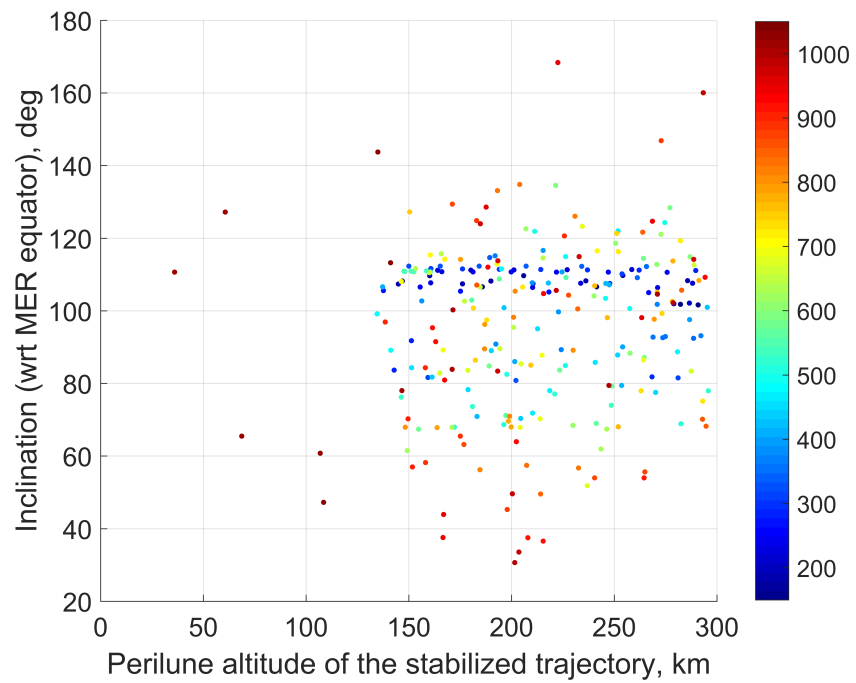


Fig. 25: Inclination and perilune altitude of stable low-perilune orbits accessible from the northern 11:3  $L_1$  NRHO and the associated total  $\Delta V$  (in m/s).

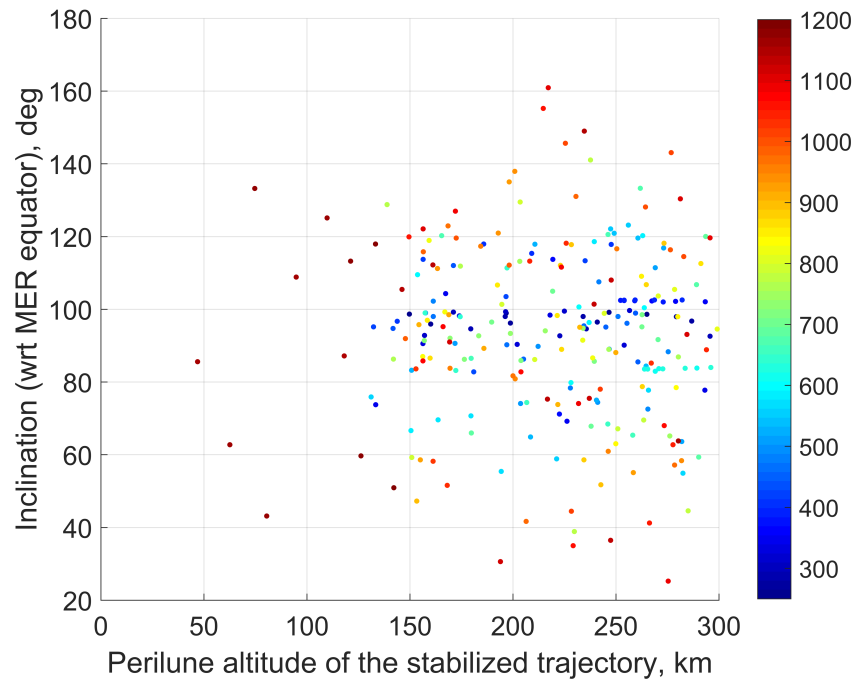


Fig. 26: Inclination and perilune altitude of stable low-perilune orbits accessible from the southern 11:3  $L_1$  NRHO and the associated total  $\Delta V$  (in m/s).

## VI. ACKNOWLEDGMENTS

This study is supported by the Russian Science Foundation grant 14-11-00621.

## REFERENCES

- [1] Lidov, M.L., A Family of Spatial Periodic Orbits Near the Moon and Planets, *Doklady Akademii Nauk SSSR*, 1977, Vol. 223, No. 6, pp. 1068–1071 (in Russian).
- [2] Breakwell, J.V. and Brown, J.V., The “Halo” Family of 3-Dimensional Periodic Orbits in the Earth-Moon Restricted 3-body Problem, *Celestial Mechanics*, 1979, Vol. 20, No. 4, pp. 389–404.
- [3] Williams, J., Lee, D.E., Whitley, R.J., et al., Targeting Cislunar Near Rectilinear Halo Orbits for Human Space Exploration, *27th AAS/AIAA Space Flight Mechanics Meeting*, San-Antonio, TX, USA, February 5–9, 2017, Paper AAS 17-267, 20 p.
- [4] Zimovan, E.M., Howell, K.C., and Davis, D.C., Near Rectilinear Halo Orbits and Their Application in Cis-Lunar Space, *3rd IAA Conference on Dynamics and Control of Space Systems* (DyCoSS), Moscow, Russia, May 30–June 1, 2017, Paper IAA-AAS-DyCoSS3-125, 20 p.
- [5] Wall, M., NASA Plans to Build a Moon-Orbiting Space Station: Here’s What You Should Know, <https://www.space.com/41763-nasa-lunar-orbiting-platform-gateway-basics.html> (retrieved Sep 13, 2018).
- [6] Davis, D.C., Bhatt, S.A., Howell, K.C., et al., Orbit Maintenance and Navigation of Human Spacecraft at Cislunar Near Rectilinear Halo Orbits, *27th AAS/AIAA Space Flight Mechanics Meeting*, San-Antonio, TX, USA, February 5–9, 2017, Paper AAS 17-269, 20 p.
- [7] Guzzetti, D., Zimovan, E.M., Howell, K.C., and Davis, D.C., Stationkeeping Analysis for Spacecraft in Lunar Near Rectilinear Halo Orbits, *27th AAS/AIAA Space Flight Mechanics Meeting*, San-Antonio, TX, USA, February 5–9, 2017, Paper AAS 17-395, 20 p.
- [8] Ulybyshev, Yu., Study of Optimal Transfers from L2 Halo-Orbits to Lunar Surface, *54th AIAA Aerospace Sciences Meeting*, San Diego, CA, USA, January 4–8, 2016, Paper AIAA 2016-0480, 14 p.
- [9] Parker, J.S. and Anderson, R.L., *Low-Energy Lunar Trajectory Design*, John Wiley & Sons, Inc., 2014, 448 p.
- [10] Folkner, W.M., Williams, J.G., Boggs, D.H., et al., *The Planetary and Lunar Ephemerides DE430 and DE431*, IPN Progress Report 42-196, 2014, 81 p.
- [11] Mazarico, E., Lunar Gravity Field: GRGM1200A, <https://pgda.gsfc.nasa.gov/products/50> (retrieved Sep 13, 2018).
- [12] Klumpp, A.R., Apollo Lunar Descent Guidance, *Automatica*, Vol. 10, No. 3, 1975, pp. 133–146.
- [13] Citron, S.J., Dunin, S.E., and Meissinger, H.F., A Terminal Guidance Technique for Lunar Landing, *AIAA Journal*, 1964, Vol. 2, No. 3, pp. 503–509.
- [14] McInnes, C.R., Path Shaping Guidance for Terminal Lunar Descent, *Acta Astronautica*, 1995, Vol. 36, No. 7, pp. 367–377.
- [15] Chomel, C.T. and Bishop, R.H., Analytical Lunar Descent Guidance Algorithm, *Journal of Guidance, Control, and Dynamics*, 2009, Vol. 32, No. 3, pp. 915–926.
- [16] Lawden, D.F., *Optimal Trajectories for Space Navigation*, Butterworths, London, 1963, 126 p.
- [17] Rea, J.R., *An Investigation of Fuel Optimal Terminal Descent*, Ph.D. Thesis, University of Texas at Austin, 2009, 351 p.

- [18] Li, M.D., Macdonald, M., McInnes, C.R., and Jing, W.X., Analytical Landing Trajectories for Embedded Autonomy, *Proceedings of the Institution of Mechanical Engineers, Part G: Journal of Aerospace Engineering*, 2010, Vol. 224, Issue 11, pp. 1177–1191.
- [19] Leeghim, H., Cho, D.-H., and Kim, D., An Optimal Trajectory Design for the Lunar Vertical Landing, *Proceedings of the Institution of Mechanical Engineers, Part G: Journal of Aerospace Engineering*, 2016, Vol. 230, Issue 11, pp. 2077–2085.
- [20] Azimov, D.M. and Bishop, R.H., Integrated Targeting and Guidance for Powered Planetary Descent, *Journal of the Astronautical Sciences*, 2018, Vol. 65, Issue 2, pp. 229–259.
- [21] Cho, D.-H., Jeong, B., Lee, D., and Bang, H., Optimal Perilune Altitude of Lunar Landing Trajectory, *International Journal of Aeronautical and Space Sciences*, 2009, Vol. 10, No. 1, pp. 67–74.
- [22] Hawkins, A.M., *Constrained Trajectory Optimization of a Soft Lunar Landing from a Parking Orbit*, Master Thesis, Massachusetts Institute of Technology, 2005, 144 p.
- [23] Lu, P., Propellant-Optimal Powered Descent Guidance, *Journal of Guidance, Control, and Dynamics*, 2018, Vol. 41, No. 4, pp. 813–826.
- [24] Ploen, S., Acikmese, B., and Wolf, A., A Comparison of Powered Descent Guidance Laws for Mars Pinpoint Landing, *AIAA/AAS Astrodynamics Specialist Conference and Exhibit*, Keystone, CO, USA, August 21–24, 2006, Paper AIAA 2006-6676, 16 p.
- [25] Acikmese, B. and Ploen, S.R., Convex Programming Approach to Powered Descent Guidance for Mars Landing, *Journal of Guidance, Control, and Dynamics*, 2007, Vol. 30, No. 5, pp. 1353–1366.